Crystal structure, growth and characterizations of a novel organic third-order nonlinear optical crystal: guanidinium cinnamate

M. Dhavamurthy[1] · R. Raja[1] · K. Syed Suresh Babu[2] · R. Mohan[1]

Abstract Guanidinium cinnamate (GUCN), a single crystal, was grown by slow evaporation technique. Single-crystal X-ray diffraction study revealed that GUCN crystal belongs to monoclinic crystal system with the space group $P2_1/c$. Thermal studies revealed that the GUCN is thermally stable up to 238 °C. The optical transmittance studies were carried out for the crystal, and the lower cutoff wavelength of the grown crystal was observed at 322 nm. The luminescent study showed that the GUCN crystal has high degree of luminescence. Third-order nonlinear refractive index n_2, nonlinear absorption coefficient β and susceptibility $\chi^{(3)}$ parameters were estimated by Z-scan technique. The four independent tensor coefficients ε_{11}, ε_{22}, ε_{33} and ε_{13} of dielectric permittivities for monoclinic GUCN were calculated. The mechanical properties of the grown crystals were studied using Vickers micro-hardness tester at different planes.

1 Introduction

The nonlinear optical properties of molecules and their hyper-polarizabilities have become an important area of extensive research. A lot of experimental [1] and theoretical [2, 3] efforts are focused on the study of bulk NLO properties as well as their dependence on the first-order hyper-polarizabilities of molecules. The delocalized electronic structure of π-conjugated organic compound offers a number of tempting opportunities in applications of NLO materials. Recently, the scope for the synthesis and characterization of third-order organic materials has expanded considerably. The microscopic theoretical models predict large non-resonant third-order optical nonlinearity, which is associated with delocalized π-electron systems. Therefore, no particular bulk symmetry is required for nonzero $\chi^{(3)}$. A crystalline medium in which the molecules align in the same direction has a larger $\chi^{(3)}$ value [4–6]. Our interest is to develop molecular and crystal design technique for assembling such materials. In particular, organic systems provide many interesting structure and bonding schemes for the molecular engineering of new materials.

Cinnamic acid, a derivative of phenylalanine, composes a relatively large family of organic isomers [7, 8]. In nature, cinnamic acid derivatives are important metabolic building blocks in the production of lignins for higher plants. The carboxylic group is separated from the aromatic ring by a double bond in the structure of cinnamic acid. It causes conjugation between the C=C and the π-electron system. Single crystals of mercury cinnamate were grown using acetone as solvent by slow evaporation growth method by Ravindran et al. [9]. The SHG efficiency of the compound was found to be high, and the crystal has thermal stability up to 289.8 °C. Janos Erostyak et al. reported the interesting luminescence features of mixed complexes of europium and gadolinium with cinnamic acid (Eu/Gd/CA) [10]. The luminescence properties of the samples studied in powder form are determined by both intra- and intermolecular energy transfer processes. After the detailed analyses of the earlier studies on cinnamate derivatives, an attempt is made in the present study to synthesize and grow a single crystal of guanidinium cinnamate. The characteristics studies such

✉ R. Mohan
professormohan@yahoo.co.in

1 Department of Physics, Presidency College, Chennai 600005, India

2 Department of Physics, The New College, Chennai 600014, India
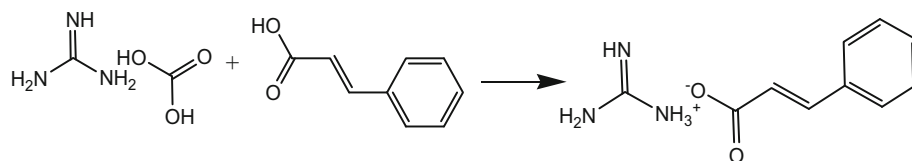
as single-crystal XRD, thermal, optical and mechanical properties are taken of the grown guanidinium cinnamate crystals.

2 Experimental

2.1 Material synthesis and crystal growth

Guanidinium cinnamate (GUCN) was synthesized by taking equimolar quantities of guanidine carbonate and cinnamic acid in deionized water. A transfer of proton from the electron-donor group of an acid to the electron acceptor group of a base results in an enhancement of hyper-polarizability in the compound. Figure 1 represents the reaction scheme for the formation of the title complex. There is intermolecular hydrogen bonding between amino group of guanidinium cation and carboxylate group of cinnamate anion. The amino 'N' atom of the guanidinium cation forms N–H…O hydrogen bonds with the O-atoms of the carboxylate anion.

The synthesized salt was recrystallized four times before growth. Transparent tiny crystals with well–defined shape and free from visible inclusions were chosen as the seed crystal. Single crystal of GUCN was grown from saturated aqueous solution (pH 7.5) of the synthesized salt by slow evaporation solution growth technique at 30 °C using a constant temperature bath having a control accuracy of ±0.01 °C. A single crystal of size $10 \times 8 \times 6$ mm^3 was grown in a period of 35–45 days. The image of the grown crystals of GUCN is shown Fig. 2.
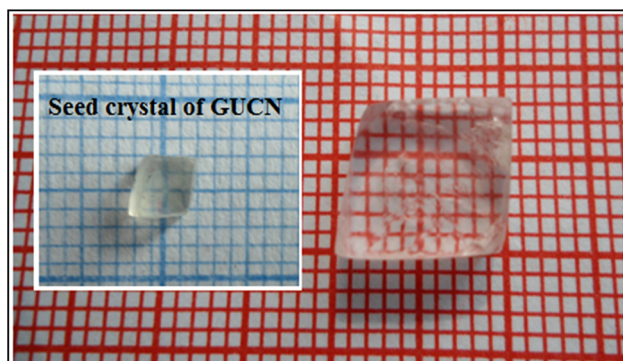

Fig. 2 As-grown crystal of GUCN crystal

3 Characterizations

3.1 Single-crystal X-ray diffraction analysis

Guanidinium cinnamate, $CH_6N_3^+$ $C_9H_7O_2^-$, synthesized at 293 K, forms a primary hydrogen-bonded ribbon structure through cyclic hydrogen bonding interactions involving all six protons of the guanidinium cation with the amino N-atom and carboxylate O-atom acceptors of the anion. The Bruker Kappa APEXII [11] single-crystal X-ray diffractometer with MoKα ($\lambda = 0.71073$ Å) radiation was used. The structure was solved by direct methods using the program SHELXS-97 and refined by full-matrix least-squares method using SHELXL-97 [12]. The crystallographic data of the title compound are listed in Table 1. The new crystal structure data have been deposited in the Cambridge Crystallography Data center with number 1054453.

The R value of the full-matrix least-squares refinement is given in Table 1. The guanidinium cinnamate ($C_{10}H_{13}N_3O_2$) crystallizes in the monoclinic space group P21/c with unit cell parameters $a = 7.443(8)$ Å, $b = 20.453(2)$ Å, $c = 7.852(10)$ Å, $\alpha = 90°, \beta = 91.573(4)°, \gamma = 90°, Z = 4$, and cell volume $= 1051.7(1)$ Å^3. X-ray analysis confirms the molecular structure and interatomic distance as shown in Fig. 3. The toluene ring (C1–C6) is almost planar with least-squares planes of the methane-diamine ring, making dihedral angle of 78.8(3)°. Toluene ring has the largest deviation from the mean plane (0.027 Å) for C7 atom. The toluene group (C6–C9) is slightly twisted from the attached toluene ring with the torsion angle C6–C7–C8–C9 = 178.5(4)°. In the crystal, molecules are linked via N–H…O hydrogen bonds (Table 2), forming infinite bonds lying parallel to (1 1 0) and composed of alternate R_2^2 (6) graph-set ring motifs. The crystal packing is further stabilized by π–π* intermolecular interactions [centroid–centroid distance = 4.575 Å]. In the crystal packing structure (Fig. 4), all guanidinium hydrogen atoms are packed through intermolecular hydrogen bonds. The morphology of parallelogram-shaped GUCN crystal with six symmetrical faces is shown in Fig. 5. The major flat face along b-axis was indexed as (0 1 0) plane, and the other planes in the crystals were indexed as (0 −1 0), (1 0 −1), (−1 0 1), (1 0 1), and (−1 0 −1). From Fig. 5, it is clear that the (0 1 0) plane has larger area due to the reduced growth rate along crystallographic b-direction compared to a-direction and c-direction.

Table 1 Crystal data and structure refinement for GUCN crystal

Empirical formula	$C_{10} H_{13} N_3 O_2$	
Formula weight	207.23	
Temperature	293 (2) K	
Wavelength	0.71073 Å	
Crystal system, space group	Monoclinic	$P2_1/c$
Unit cell dimensions	$a = 7.4437(8)$ Å	$\alpha = 90°$
	$b = 20.453(2)$ Å	$\beta = 91.573(4)°$
	$c = 7.8525(10)$ Å	$\gamma = 90°$
Volume	1195.1(2) Å^3	
Z, calculated density	4, 1.169 Mg m^{-3}	
Absorption coefficient	0.083 mm^{-1}	
F(000)	452	
Crystal size	$6 \times 10 \times 22$ mm^3	
Theta range for data collection	1.99–24.98°	
Limiting indices	$-8 \leq h \leq 6, -24 \leq k \leq 24, -9 \leq l \leq 9$	
Reflections collected/unique	18670/2095 [R(int) = 0.0362]	
Completeness to $\theta = 24.98$	99.7 %	
Refinement method	Full-matrix least-squares on F^2	
Data/restraints/parameters	2095/0/136	
Goodness of fit on F^2	1.073	
Final R indices [I > 2sigma(I)]	$R1 = 0.0878, wR_2 = 0.2626$	
R indices (all data)	$R1 = 0.1448, wR_2 = 0.3367$	

Fig. 3 ORTEP diagram of GUCN crystal; displacement ellipsoids are drawn at 50 % probability level
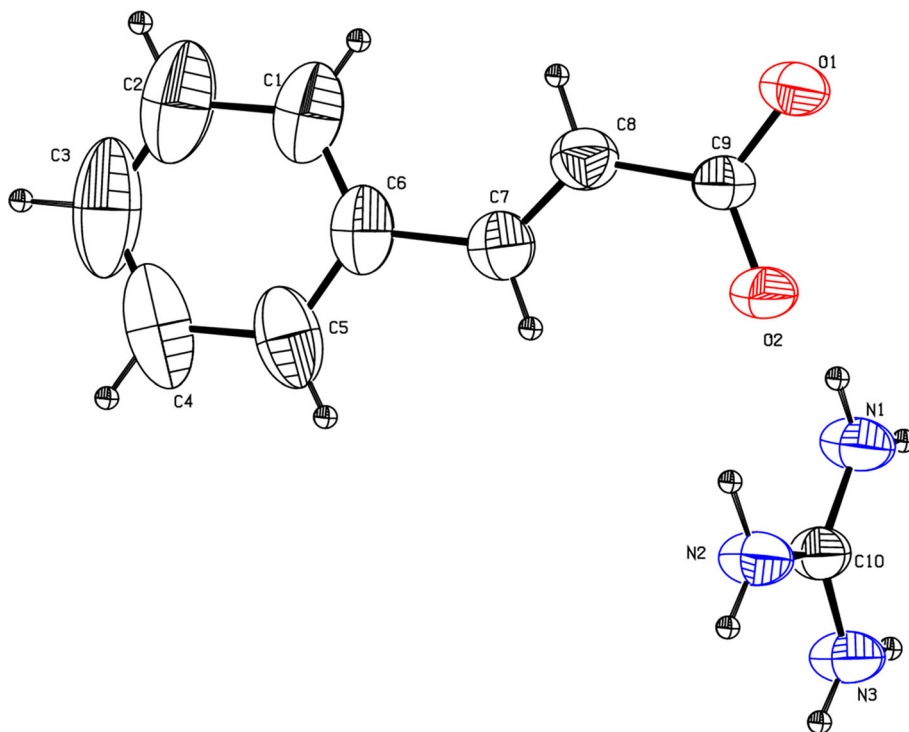
3.2 Thermal analysis

Thermo gravimetric analysis (TGA) and differential thermal analysis (DTA) were performed with a NETZSCH STA 409 PC/PG analyzer in the nitrogen atmosphere. The samples were placed in a platinum crucible and heated from room temperature to 500 °C at a rate of 10 °C/min. The GUCN sample weighing

Table 2 Hydrogen bonds in GUCN crystal with bond distances and bond angle

| Hydrogen bond	Bond distance (Å)		Bond angle	
D-H…A	d(D-H)	d(H…A)	d(D…A)	<(DHA)°
N1–H1A…O1	0.97	1.84	2.811 (5)	173
N2–H2A…O1	0.83	2.13	2.858 (5)	146
N3–H3A…O1	0.82	2.13	2.885 (4)	153
N3–H3B…O2	1.00	1.83	1.825 (5)	177

Symmetry codes: (i) $-1/2 + x$, $½ - y$, $-1/2 + z$ (ii) $x, y, -1 + z$

4.919 mg was taken for the measurement, and the thermogram is illustrated in Fig. 6. The material was moisture-free and was thermally stable up to 238 °C, and the sharp endothermic peak in DTA at 241 °C indicates the melting point of the material. The DTA revealed exactly the same changes shown by the TGA. Since there was no endothermic or exothermic transition below 200 °C, the material is proved to be stable in this region. In the DTA curve, first endothermic peak appears at 241 °C indicating the melting point of grown crystal. The TGA plot shows the softening of GUCN crystal between 255 and 473 °C accompanied by the loss of weight of about 75.5 %. This weight loss is due to the release or elimination of NH_3, CO_2 and H_2O molecules. The broad endothermic peak at 292 °C in DTA is found to be matching with the corresponding weight loss in TGA curve, which is attributed to the energy required for the release of the gaseous molecules. The final residue weight left was about 27.02 % after heating to 500 °C.
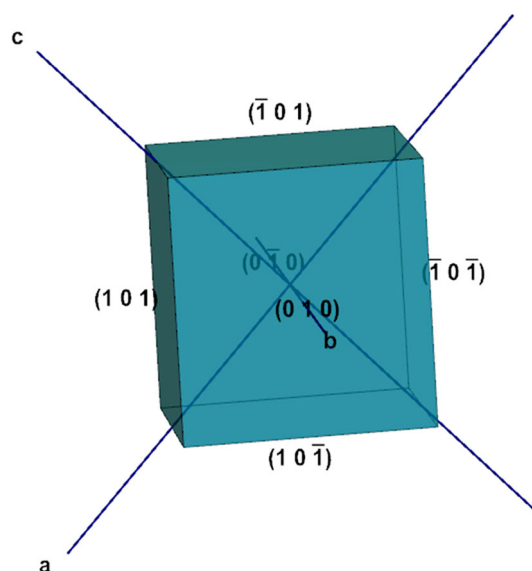
Fig. 5 Morphology structure of GUCN crystal

3.3 UV–Vis–NIR spectra analysis

The UV–Vis–NIR transmittance spectrum of the (0 1 0) plane of GUCN crystal was recorded using a Shimadzu UV–Vis–NIR spectrophotometer in the wavelength range of 200–900 nm (Fig. 7). From the spectrum, it was noted that the UV transparency cutoff occurs at 322 nm, and there was no remarkable absorption in the entire region of the spectra. The transmittance of GUCN in (0 1 0) plane is about 75–80 %, which is good enough for the generation of higher harmonic light using infrared lasers through NLO phenomena. Since the crystal was transparent in the whole
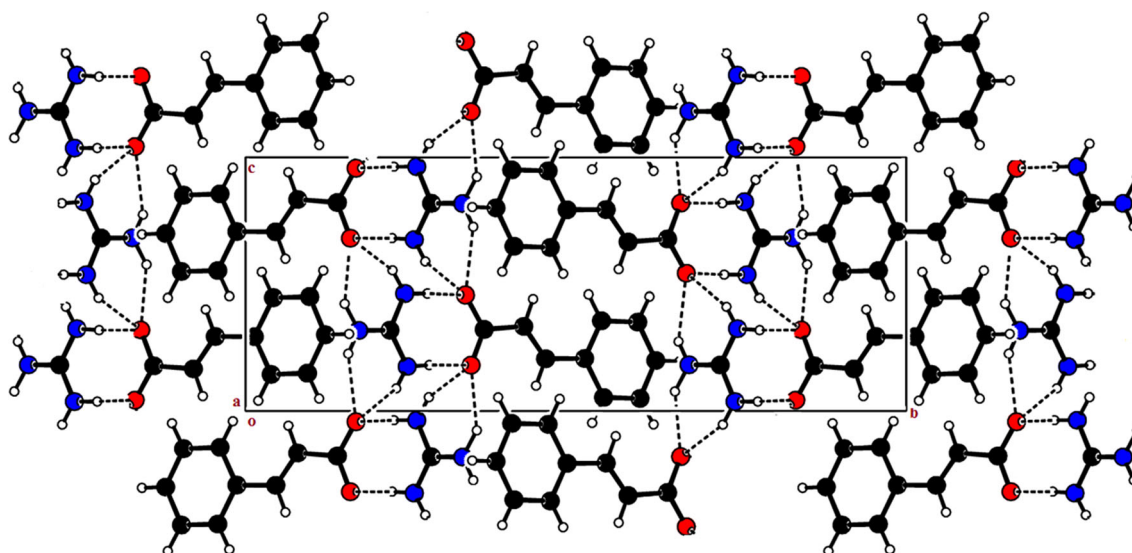
Fig. 4 Packing diagram of GUCN viewed down the *a*-axis. *Dashed lines* indicate intermolecular N–H…O hydrogen bonds
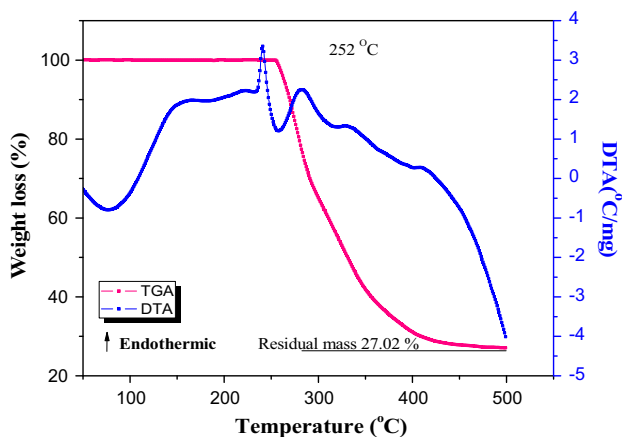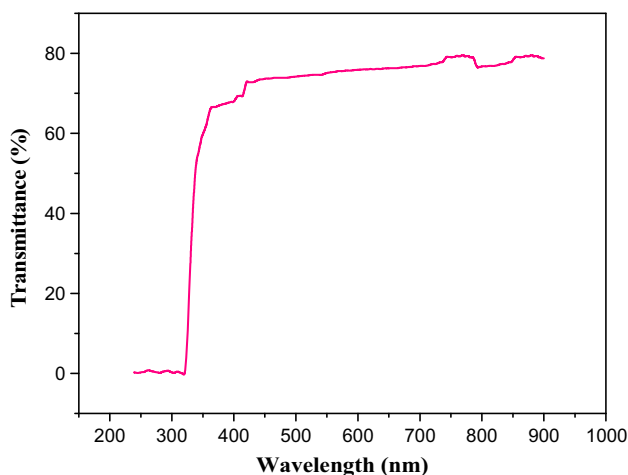
Fig. 6 TG-DTA diagram of GUCN crystal

Fig. 7 UV–Vis–NIR transmission spectrum of GUCN crystal
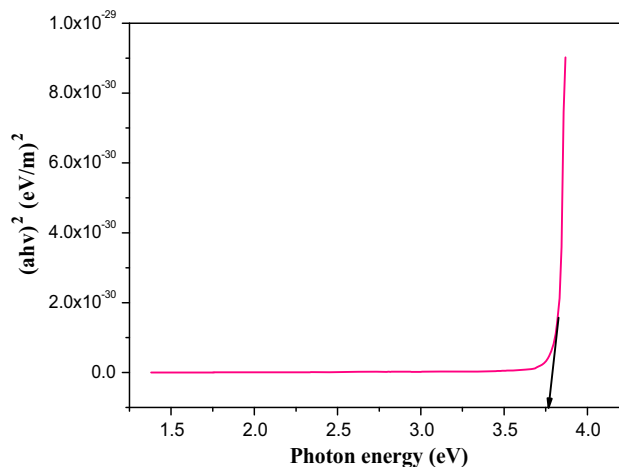

Fig. 8 Plot of $(\alpha h v)^2$ versus photon energy of GUCN crystal

Fig. 8, and E_g can be evaluated by extrapolation of the linear part. The optical band gap energy is found to be 3.6 eV. The obtained result is analogous to the band gap energy $E_g = 3.73$ eV estimated for guanidinium 4-aminobenzoate crystal whose cutoff wavelength is 330 nm [14].

3.4 Photoluminescence

Photoluminescence (PL) spectrum was carried out using a Varian Cary Eclipse Fluorescence spectrophotometer with a xenon flash lamp as the excitation source at a scan speed of 600 nm/min, having filter size of 5 nm. The emission spectrum was recorded in the wavelength range 300–650 nm, and the GUCN powder sample was excited at the wavelength of 300 nm in solid phase, whose UV cutoff wavelength is 320 nm. The emission spectrum is shown in Fig. 9. From the figure, it was observed that the emission peak of GUCN occurs at 410 nm. This indicates that the grown crystals have a violet fluorescence emission. The prime impact of COO^- ions of the cinnamic acid was to influence on the formation of highest molecular orbital (HOMO) state, whereas the lowest unoccupied molecular orbital (LUMO) state comes from the NH^+ ions of guanidinium. During the interband transition, the electron looses its energy in the form of vibrational mode in the crystal; this energy lost contributes to the luminescence phenomena.

3.5 Third-order nonlinear optical effect

The third-order nonlinear susceptibility, nonlinear refractive index (n_2) and the nonlinear absorption coefficient (β) of GUCN crystals were evaluated from the measurements of Z-scan using 632.8-nm, 6-ns Nd:YAG laser source. Open-aperture and closed-aperture Z-scan results in GUCN

region of 900–325 nm, one could use GUCN as a third harmonic generator of Nd:YAG ($\lambda = 1064$ nm) laser to produce third harmonic at ~ 354.6 nm. The measured transmittance T was used to calculate the absorption coefficient (α) using the formula:

$$\alpha = (2.306/t) \log(1/T) \tag{1}$$

where t is the thickness of the sample. The absorption coefficient α of a crystalline solid obeys the following relationship [13]:

$$(\alpha h v) = A(E_g - h v)^n \tag{2}$$

where E_g is the optical energy gap and n is an exponent that characterizes the optical absorption process. For direct allowed transition, $n = 1/2$; for direct forbidden transition, $n = 3/2$; for indirect allowed transition, $n = 2$; and for indirect forbidden transition, $n = 3$. For the direct allowed transition, $(\alpha h v)^2 = A(E_g - h v)$. The variation of $(\alpha h v)^2$ versus $h v$ in the fundamental absorption region is plotted in
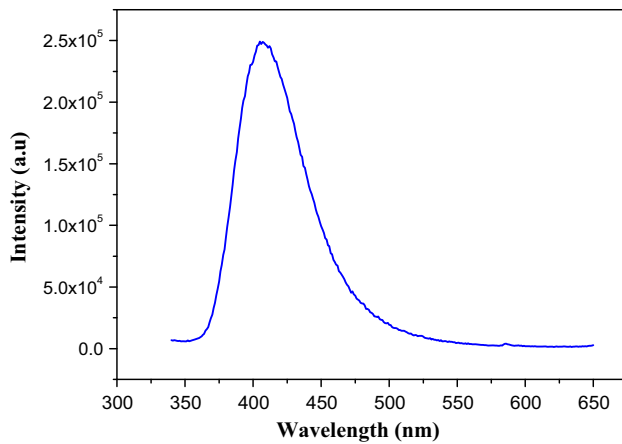
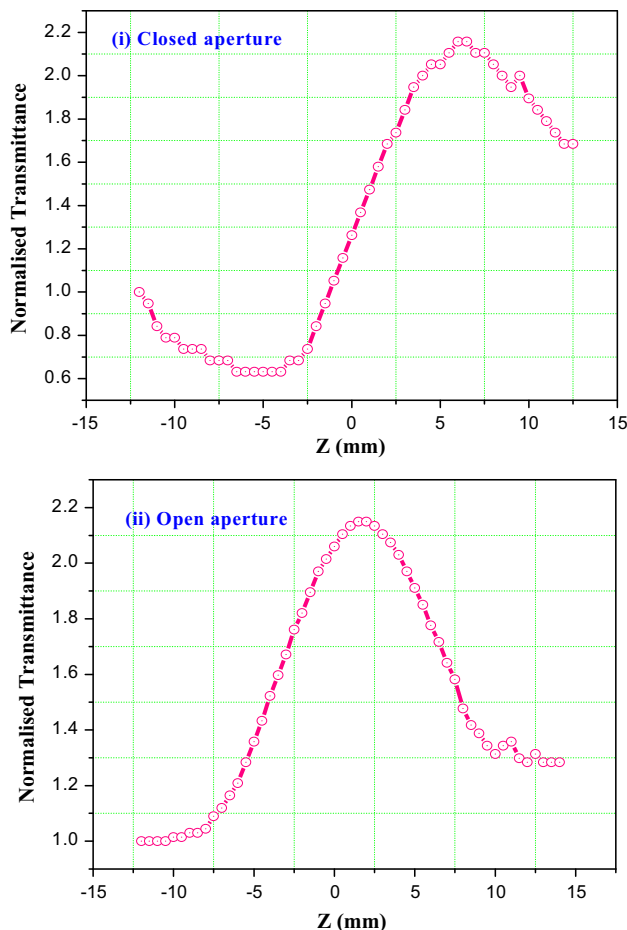Fig. 9 Photoluminescence spectrum of GUCN crystal

Fig. 10 Plot of normal transmittance with (i) closed and (ii) open apertures as a function of Z-position of GUCN crystal

crystals were used for measuring NLA coefficient and nonlinear refractive index, respectively. Figure 10 (1) shows the Z-scan data for the closed-aperture setup for

GUCN at a transmission of about 80 %. The peak followed by a valley-normalized transmittance, which is the signature for positive nonlinearity [15]. Z-scan data for the open-aperture $(S = 1)$ setup of the same specimen is illustrated in Fig. 10 (2). A spatial distribution of the temperature in the crystal surface was produced, due to the localized absorption of a tightly focused beam propagating through the absorbing sample. Hence, a spatial variation in the refractive index is produced, which acts as a thermal lens resulting in the phase distortion of the propagating beam. The on-axis phase shift $\Delta\phi$ at the focus is related to the nonlinear refractive index as

$$n_2 = \frac{\Delta\phi}{kI_oL_{eff}} \tag{3}$$

where $k = \frac{2\pi}{\lambda}$, λ is the laser wavelength, I_o is the intensity of the laser beam at the focus $(Z = 0)$. $L_{eff} = \frac{[1-\exp(-\alpha L)]}{\alpha}$ is the effective thickness of the sample, α is the linear absorption, and L is the thickness of the sample. From the open-aperture Z-scan data, the nonlinear absorption coefficient is estimated from the equation

$$\beta = \frac{2\sqrt{2}\Delta T}{I_0L_{eff}} \tag{4}$$

where ΔT is the valley value at the open-aperture Z-scan curve. The value of β will be negative for saturable absorption and positive for two-photon absorption. The real and imaginary parts of the third-order nonlinear optical susceptibility $\chi^{(3)}$ are defined by

$$\chi^{(3)} = \sqrt{(\text{Re}\chi^{(3)})^2 + (\text{Im}\chi^{(3)})^2} \text{ esu} \tag{5}$$

Table 3 interprets the experimental details and the results of the Z-scan technique for GUCN. The calculated value of the nonlinear refractive index n_2 is 1.6879×10^{-10} cm^2/W. From the open-aperture Z-scan curve, it can be concluded that as the minimum value lies near the focus $(Z = 0)$, the nonlinear absorption is regarded as two-photon absorption. The nonlinear absorption coefficient β is found to be 2.4996×10^{-5} cm/W. The third-order susceptibility $\chi^{(3)}$ of GUCN is 2.0541×10^{-8} esu.

3.6 Dielectric study

The dielectric measurement was taken using the instrument Agilent 4284-A LCR meter. The dielectric permittivity ε is a second-rank symmetric tensor. The maximum number of independent constants was six, but this number can be reduced for higher-symmetry crystals. For the monoclinic GUCN crystal, the dielectric permittivity tensor with respect to the crystallographic axes in the conventional orientation is [16],

Table 3 Measurement details and the results of the Z-scan technique for GUCN crystal

Laser beam wavelength λ	632.8 nm
Incident intensity at the focus $Z = 0$	3.13 MW/cm^2
Lens focal length f	12 cm
Optical path distance Z	115 cm
Beam radius of the aperture ω_a	1 cm
Aperture radius of detector r_a for closed	4 mm
Sample thickness L	0.95 mm
Effective thickness L_{eff} of sample	0.779 mm
Linear transmittance S	0.2738
Nonlinear refractive index n_2	1.68793×10^{-10} cm^2/W
Nonlinear absorption coefficient β	2.4996×10^{-5} cm/W
Third-order susceptibility $\chi^{(3)}$	2.05418×10^{-8} esu

$$\begin{bmatrix} \varepsilon_{11} & 0 & \varepsilon_{13} \\ 0 & \varepsilon_{22} & 0 \\ \varepsilon_{31} & 0 & \varepsilon_{33} \end{bmatrix} \tag{6}$$

There are four independent principal dielectric components, $\varepsilon_{11}, \varepsilon_{31} (= \varepsilon_{13}), \varepsilon_{22}$ and ε_{33}. To determine these values for the grown crystal, the samples were obtained by cutting the crystal along four different orientations. Dielectric permittivities $\varepsilon_{11}, \varepsilon_{22}, \varepsilon_{33}$ were determined from the a-, b- and c-cut samples as shown in Fig. 11. The sample was electroded on either side with graphite coating in order to make it work like a parallel-plate capacitor. The dielectric tensor for GUCN single crystal was determined as a function of frequency at a temperature of 40 °C.

The dielectric permittivity values of the a-axis-, b-axis- and c-axis-cut samples vary with respect to frequency with differently cut samples in the range 739.21–190.606 (a-
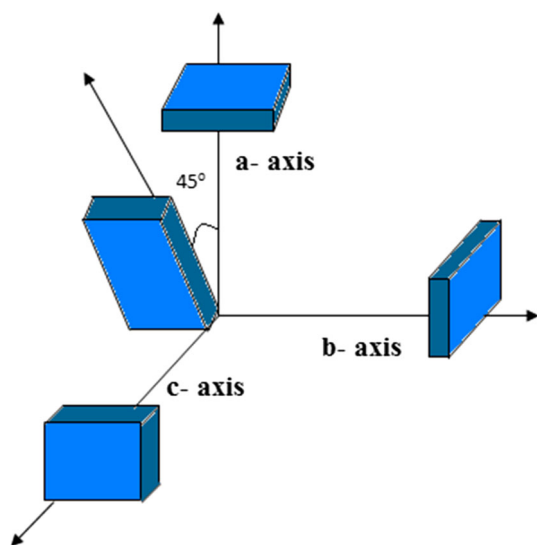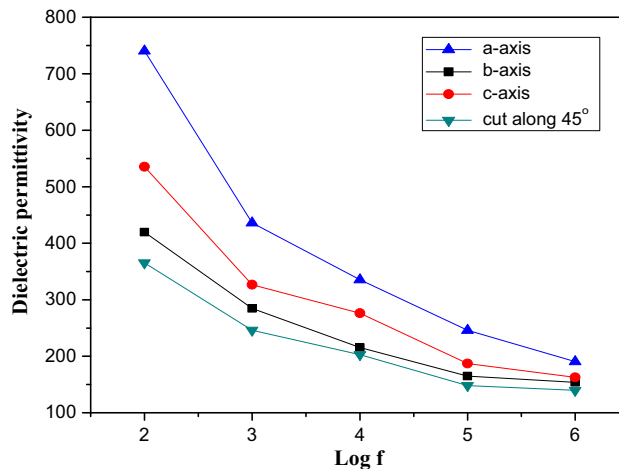

Fig. 11 Sample for dielectric study

Fig. 12 Plot of log f versus dielectric permittivity for GUCN crystal

cut), 418.45–153.98 (b-cut) and 535.43–162.87 (c-cut), respectively. The variation in dielectric permittivities as a function of frequency is shown in Fig. 12. The dielectric permittivity ε_{13} was obtained using the formula [17]:

$$\varepsilon'_{33} = \varepsilon_{11} \sin^2 \theta + 2\varepsilon_{13} \sin \theta \cos \theta + \varepsilon_{33} \cos^2 \theta \tag{7}$$

where ε'_{33} is the dielectric permittivity for the sample (cut at 45°), and its value varies from 365.34 to 139.87 with respect to the frequency shown in Fig. 12. ε_{11} and ε_{33} are the dielectric permittivity values for a-cut and c-cut crystal, respectively. The dielectric permittivity ε_{13} is found to be −272.08 for 100 Hz. The negative value of ε_{13} indicates that the dielectric polarization occurs in the negative direction of the Z-axis when an electric field is applied along the positive direction of the X-axis. The dielectric loss values are evaluated in the frequency range 100 Hz–1 MHz at the temperature of 40 °C (Fig. 13). The dielectric loss of grown crystal has a high value of 3.3 at 100 Hz and decreases to 0.7 at 1 MHz for c-cut crystal. Low value of dielectric loss indicates that the GUCN crystal contains minimum defects.

3.7 Micro-hardness study

The micro-hardness measurement on well-polished (0 1 0), (1 0 1) and (−1 0 1) planes of GUCN crystal was taken using an Economet VH 1MD micro-hardness tester with a diamond pyramidal indenter. The diagonal length of the indentation for various applied loads in gram was measured for a constant indentation period of 10 s. The indented impressions were approximately square in shape. The shape of the impression was structure dependent, face dependent and also material dependent [18]. The applied load varied from 1 to 300 g. The Vickers hardness number was obtained using the expression
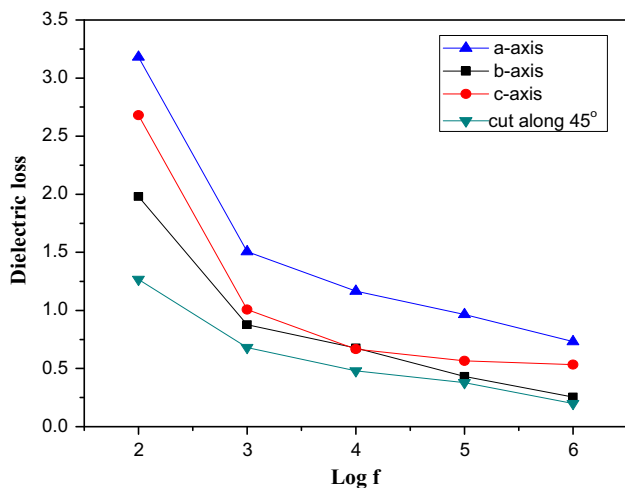
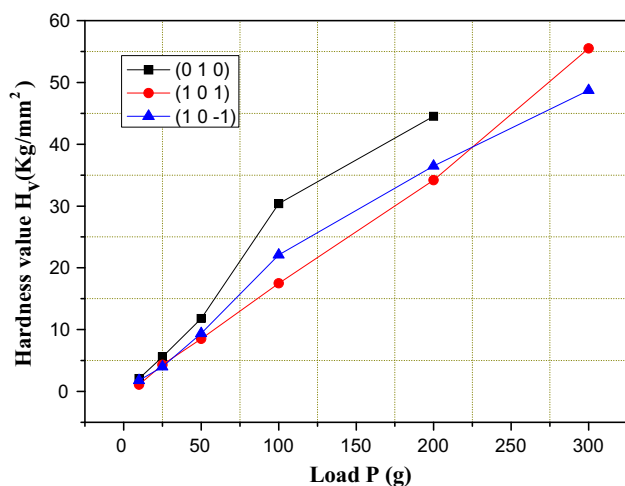**Fig. 13** Plot of log f versus dielectric loss for GUCN crystal

Fig. 14 Plot of load P versus hardness number H_v for various planes of GUCN crystal

$$H_v = 1.8544 \left(\frac{P}{d^2} \right) \text{kg/mm}^2 \qquad (8)$$

where P is the load in g and d is the average diagonal length of the indentation in mm. The variation of hardness with the applied load on the three different planes is shown in Fig. 14. Examination of the indented surface of the sample reveals the appearance of multiple cracks around indentations when P was greater than 200 g for (0 1 0) plane, and 300 g for (1 0 1) and (1 0 −1) planes, due to the release of internal stresses generated locally by indentation [19]. The phenomenon of dependence of micro-hardness of a solid on the applied load, at low level of testing, is known as indentation size effect (ISE). The micro-hardness observations showed that hardness increased with increase in load, which confirms the reverse indentation size effects

of the crystal. Meyer's index number was calculated from the Meyer's law [20], which relates the load and indentation diagonal length as

$$\log P = \log K_1 + n \log d \qquad (9)$$

where K_1 is the material constant and n is Meyer's index. Thus, a plot of log P versus log d gives a straight line, and the slope of which gives the value of 'n,' which is the work hardening coefficient. H_v should increase with the increase in P if $n > 2$ and decrease if $n < 2$. The 'n' value obtained from the plot is almost agreeable with the experimental value. According to Onitsch [21], n should lie between 1 and 1.6 for harder materials and above 1.6 for softer materials. The calculated 'n' values of GUCN are $n_1 = 1.15$, $n_2 = 1.21$ and $n_3 = 1.18$ corresponding to (0 1 0), (1 0 1) and (1 0 −1) planes, respectively, and it categorized under hard material.

4 Conclusions

An optical-quality guanidinium cinnamate (GUCN), a single crystal of dimensions $10 \times 8 \times 6 \text{ mm}^3$, was successfully grown at pH of 7.5 by the slow evaporation technique. Crystal structure and morphology of the GUCN crystal have been analyzed by XRD analysis, and the results shows that the crystal belongs to the monoclinic system with space group P2$_1$/c. The thermal behavior of GUCN crystal was studied by using TG-DTA, and it was found that the grown crystals are thermally stable up to 238 °C. Optical study revealed the cutoff wavelength of the crystal is at 322 nm in UV region with increased transparency in entire visible region. The emission peak at 410 nm revealed the material's fluorescence property in the violet wavelength region. The four dielectric tensor components were measured at a frequency of 100 Hz and at a temperature of 40 °C. Low value of dielectric loss suggests that the GUCN crystal possesses enhanced optical quality with low density of defects. The third-order nonlinear optical susceptibility, refractive index and absorption coefficient of GUCN were determined by Z-scan technique. Vickers hardness values measured on various planes reveal that GUCN was a hard material.

References

1. A. Sukhorukov, A. Kivshar, S.J. Yu, Opt. Soc. Am. B **19**(4), 772 (2002)
2. G. Maroulis, J. Mol. Struct. **633**(2–3), 177 (2003)

3. W.A. Schoonveld, J. Wildeman, D. Fichou, P.A. Bobbert, B.J. Van Wees, T.M. Klapwijk, Nature **404**, 977 (2000)
4. J.L. Moigne, L. Oswald, F. Kajzar, A. Thierry, Nonlinear Opt. **9**, 187 (1995)
5. J. Chemla, Zyss (eds.), Nonlinear Optical Properties of Organic Molecules and Crystals (Academic Press, NewYork, Vols. 1&2 1987)
6. J.L. Moigne, F. Kajzar, A. Thierry, Macromolecules **24**, 2622 (1991)
7. W. Lewandowski, M. Kalinowska, H. Lewandowski, J. Inorg. Biochem. **99**, 1407 (2005)
8. M.G.I. Hetrog, D. Kromhout, C. Aravanis, Arch. Intern. Med. **155**(4), 381 (1995)
9. B. Ravindran, G. Madhurambal, M. Mariappan, K. Ramamurthi, S.C. Mojumdar, J. Therm. Anal. Calorim. **104**, 909 (2011)
10. J. Erostyak, A. Buzady, I. Hornyak, L. Kozma, A Chem. **115**, 21 (1998)
11. A.P.E.X. Bruker, *SADABS and SAINT* (Bruker AXS Inc, Madison, 2008)
12. G.M. Sheldrick, Acta Cryst. **A64**, 112 (2008)
13. I. Watanbe, T. Okumura, J. Appl. Phys. **25**, 1851 (1986)
14. T. Arumanayagam, P. Murugakoothan, Mater. Lett. **65**, 2748 (2011)
15. S. Shettigar, G. Umesh, K. Chandrasekaran, B. Kalluraya, Synth. Met. **157**, 142 (2007)
16. T. Chen, Z. Sun, C. Song, Y. Ge, J. Luo, W. Lin, M. Hong, Cryst. Growth Des. **12**(5), 2673 (2012)
17. F. Yu, S. Zhang, X. Zhao, D. Yuan, C.M. Wang, T.R. Shrout, Cryst. Growth Des. **10**, 1871 (2010)
18. S. Suresh, A. Ramanand, D. Jayaraman, Opt. Electron. Adv. Mater. **4**, 1987 (2010)
19. B.W. Mott, *Microindentation Hardness Testing* (Butterworths, London, 1966)
20. M. Rajalakshmi, R. Indirajith, M. Palanichamy, R. Gopalakrishnan, Spectrochim. Acta, Part A **84**, 43 (2011)
21. E.M. Onitsch, Mikroskopie **2**, 131 (1947)